

Subgrid parameterizations of ocean mesoscale eddies based on Germano decomposition

Pavel Perezhogin^{1,2}, Andrey Glazunov²

¹Courant Institute of Mathematical Sciences, New York University, New York, NY, USA

²Marchuk Institute of Numerical Mathematics, Russian Academy of Sciences, Moscow, Russia

Key Points:

- We propose a three-component subgrid model consistent with the physics of 2D fluids using Germano (1986) decomposition
- The new subgrid model accurately predicts the spectral transfer of energy and enstrophy and improves a posteriori experiments
- A backscattering component (Reynolds stress) improves coarse-grid ocean models based on QG and primitive equations

arXiv:2304.06789v1 [physics.ao-ph] 13 Apr 2023

Abstract

Ocean models at intermediate resolution ($1/4^\circ$), which partially resolve mesoscale eddies, can be seen as Large eddy simulations (LES) of the primitive equations, in which the effect of unresolved eddies must be parameterized. In this work, we propose new subgrid models that are consistent with the physics of two-dimensional (2D) flows. We analyze subgrid fluxes in barotropic decaying turbulence using Germano (1986) decomposition. We show that Leonard and Cross stresses are responsible for the enstrophy dissipation, while the Reynolds stress is responsible for additional kinetic energy backscatter. We utilize these findings to propose a new model, consisting of three parts, that is compared to a baseline dynamic Smagorinsky model (DSM). The three-component model accurately simulates the spectral transfer of energy and enstrophy and improves the representation of kinetic energy (KE) spectrum, resolved KE and enstrophy decay in a posteriori experiments. The backscattering component of the new model (Reynolds stress) is implemented both in quasi-geostrophic and primitive equation ocean models and improves statistical characteristics, such as the vertical profile of eddy kinetic energy, meridional overturning circulation and cascades of kinetic and potential energy.

Plain Language Summary

Ocean models at intermediate resolution contain missing physics term that accounts for the contribution of unresolved mesoscale eddies, which needs to be parameterized. Mesoscale eddies obey complex physics which should be accounted for when proposing a parameterization. Here we consider the interscale transfer of kinetic energy and enstrophy in a barotropic fluid and propose new subgrid models which capture this transfer. Our strategy is to split the subgrid contribution into three parts and propose a model for each term separately. This approach results in excellent a priori performance and improves online simulations. We demonstrate that our analysis of subgrid fluxes generalizes well across flow regimes: the new parameterization of energy redistribution improves barotropic, quasi-geostrophic and primitive equation ocean models.

1 Introduction

The horizontal resolution of the ocean component of climate models has increased recently from non-eddy resolving resolution (around 1°) to eddy-permitting resolution (around $1/4^\circ$, Haarsma et al. (2016)). At this resolution, ocean models do resolve the largest mesoscale eddies but still fail to resolve a substantial part of the mesoscale eddy field. Consequently, such resolutions are often referred to as "grey zone" (Hewitt et al., 2020). Classical parameterizations of mesoscale eddies are based on the ideas of Reynolds averaging where temporal or ensemble averaging is used to diagnose the effect of eddies on the mean flow (Gent & McWilliams, 1990). Reynolds averaging is suitable for very coarse ocean models; however, in the grey zone, the Large eddy simulation (LES) approach is preferable (Fox-Kemper & Menemenlis, 2008; Nadiga, 2008; Graham & Ringler, 2013; Bachman et al., 2017). In the LES framework, the effect of unresolved eddies is diagnosed with a spatial filter and referred to as a subgrid forcing (Zanna & Bolton, 2020). This forcing needs to be parameterized with a subgrid model. Recently many new parameterizations of mesoscale eddies were built based on the spatial filtering approach (Nadiga, 2008; Frederiksen et al., 2012; San et al., 2013; Mana & Zanna, 2014; Bachman et al., 2017; Pearson et al., 2017; Maulik & San, 2016, 2017b; Khani et al., 2019; Khani & Dawson, 2023; Bolton & Zanna, 2019; Zanna & Bolton, 2020; Guillaumin & Zanna, 2021).

The LES approach has a long history of successful applications in three-dimensional (3D) turbulence (Sagaut, 2006) and comprises a multitude of methods. The most pop-

ular subgrid model is the Smagorinsky (1963) model which relates the subgrid fluxes to the strain rate tensor. This model belongs to a class of so-called "functional models" (Sagaut, 2006). Functional models are designed to represent the mean effect of the eddies on the resolved flow. An alternative approach to subgrid modeling is "structural modeling" (Sagaut, 2006). Structural models utilize formal series expansion to approximate the subgrid forcing. Various approximations of subgrid forcing were proposed over the years: from Velocity gradient models (VGM, Clark et al. (1979)) to Scale-similarity models (SSM, Bardina et al. (1980); Bardino et al. (1983)) and Approximate deconvolution models (ADM, Stolz et al. (2001)).

A linear combination of structural and functional models is referred to as a "mixed model" (Meneveau & Katz, 2000). Mixed models combine the best of both approaches: the structural part provides high correlation with the subgrid forcing and the functional part ensures the numerical stability of the simulations. Such mixed models can be naturally studied in the framework of Germano (1986) decomposition, where the subgrid stress is decomposed into Leonard, Cross and Reynolds stresses. Separate functional or structural models for each one of these stress terms are then proposed (Horiuti, 1997). We also mention another popular subgrid model in 3D LES: the "dynamic model" of Germano et al. (1991) which allows the estimation of the eddy viscosity coefficient directly from the resolved flow.

Quantifying the extent to which ocean models can benefit from the methods developed for 3D LES simulations is an open question. For example, subgrid parameterizations in 3D turbulence are mainly suited to simulate energy dissipation by the subgrid eddies (Meneveau & Katz, 2000). However, in quasi-2D flows, the energy cascade has an inverse direction (Ferrari & Wunsch, 2009), and thus subgrid forcing energizes the flow on average. This effect is often referred to as a kinetic energy backscatter (KEB), see Bachman et al. (2018); Loose et al. (2023); Thuburn et al. (2014); Jansen and Held (2014); Grooms et al. (2015); Zanna et al. (2017); Juricke et al. (2020, 2023); Jansen et al. (2019); Bachman (2019).

Dynamic models similar to Germano et al. (1991) have been proposed for quasi-2D flows, see Bachman et al. (2017); Pawar et al. (2020); San (2014); Maulik and San (2017a, 2017c). These models simulate only the forward energy transfer, and consequently, their consistency with the physics of quasi-2D flows is limited. On the contrary, various structural models have been shown to simulate the backward transfer of energy, see for example Chen et al. (2003, 2006); Bouchet (2003); Nadiga (2008); Mana and Zanna (2014); Maulik and San (2017b); Anstey and Zanna (2017); Zanna and Bolton (2020); Khani and Dawson (2023). In this paper, we apply the approach of structural modeling to represent the backward energy transfer and propose new dynamic mixed models.

The existing dynamic models in quasi-2D fluids often suffer from a build-up of energy near the grid scale (Bachman et al., 2017; Maulik & San, 2017a, 2017c; Guan, Chattopadhyay, et al., 2022). This indicates that numerical effects may lead to large errors even in physically meaningful parameterizations (Ghosal, 1996; Chow & Moin, 2003). In particular, Thuburn et al. (2014) shows that the subgrid kinetic energy transfer diagnosed from the high-resolution data significantly depends on the choice of the numerical scheme. In this paper, we reduce discretization errors by leveraging an explicit filtering approach (Gullbrand & Chow, 2003; Carati et al., 2001; Winkelmann et al., 2001; Lund, 2003; Bose et al., 2010). The explicit filtering approach treats a filter width and a grid step as independent parameters. The role of discretization errors can be then reduced by enlarging a filter-to-grid width ratio (FGR, Bose et al. (2010); Sarwar et al. (2017)).

The goal of our study is to propose new subgrid momentum closures of ocean mesoscale eddies which are consistent with the physics of quasi-2D flow. We analyze the

enstrophy and energy fluxes in barotropic decaying turbulence using Germano (1986) decomposition. We show that the Leonard and Cross stresses describe the enstrophy dissipation, and Reynolds stress describes additional energy backscatter. Leonard stress can be computed directly. We propose a biharmonic Smagorinsky model for the Cross stress and a structural model for the Reynolds stress which is similar to Horiuti (1997). We estimate the Smagorinsky coefficient using the dynamic model of Germano et al. (1991). The energy flux produced by backscatter parameterization is determined by considering the budget of subgrid KE (Jansen & Held, 2014) and estimation of subgrid KE (Khani & Dawson, 2023). The resulting three-component subgrid model simulates energy and enstrophy fluxes and improves a posteriori experiments. Additionally, we show that the new backscatter model (Reynolds stress) improves quasi-geostrophic and primitive equation ocean models.

The study is structured as follows. In Section 2 we describe the governing equations. In Section 3 we analyze subgrid fluxes using Germano (1986) decomposition. In Section 4 we describe subgrid models. In Section 5 subgrid models are evaluated in a posteriori experiments. Section 6 is devoted to the implementation to more realistic ocean models.

2 Governing equations

In this section, we describe a Direct numerical simulation (DNS) of decaying barotropic turbulence and numerical schemes.

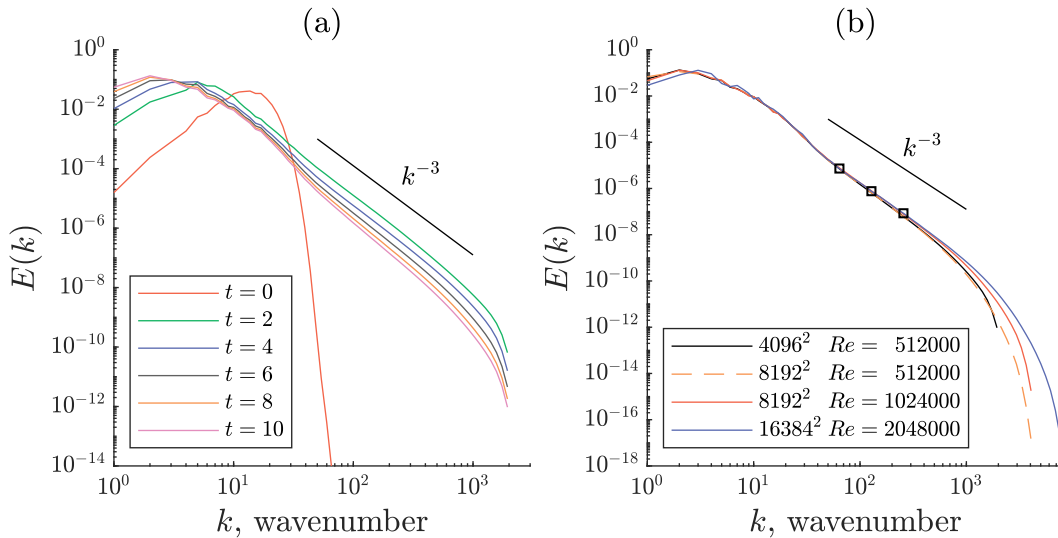


Figure 1. Kinetic energy spectrum in DNS simulations: (a) time evolution at mesh 4096^2 and $Re = 512000$, and (b) additional combinations of mesh and Reynolds number at $t = 10$. Squares show the cutoff wavenumber (π/Δ_g) , where Δ_g – grid step) for the coarse LES models at resolutions 128^2 , 256^2 and 512^2 .

The dimensionless barotropic vorticity equation in a doubly periodic domain of size $2\pi \times 2\pi$ is (Maulik & San, 2017a, 2017c; Guan, Chattopadhyay, et al., 2022):

$$\frac{\partial \omega}{\partial t} + \frac{\partial}{\partial x_j} (u_j \omega) = \frac{1}{Re} \nabla^2 \omega, \quad \nabla^2 \psi = \omega, \quad (1)$$

where x_1 and x_2 are Cartesian coordinates, $\nabla = (\partial_{x_1}, \partial_{x_2})$ is the gradient operator. We assume summation over the repeated indices ($j = 1, 2$). The relative vorticity

ω , streamfunction ψ and velocity vector components u_j are related to each other as $\omega = \partial_{x_1} u_2 - \partial_{x_2} u_1$ and $(u_1, u_2) = (-\partial_{x_2} \psi, \partial_{x_1} \psi)$. The Reynolds number is defined by dimensional RMS velocity (\tilde{u}_{rms}), domain size $2\pi\tilde{L}$ and molecular viscosity ($\tilde{\nu}$) as $Re = \tilde{u}_{\text{rms}}\tilde{L}/\tilde{\nu}$.

The turbulence is initialized with a random divergence-free flow having the following kinetic energy density (per unit wavenumber k and unit area):

$$E(k) = Ak^4 \exp(-(k/k_p)^2), \quad A = \frac{4k_p^{-5}}{3\sqrt{\pi}}, \quad (2)$$

where $k_p = 10$, $k = \sqrt{k_1^2 + k_2^2}$ and k_1, k_2 are components of wavevector. The normalization constant A is chosen to set the RMS velocity to one: $u_{\text{rms}} = (2 \int E(k) dk)^{1/2} = 1$. We integrate equations (1) with initial perturbation of form (2) until the dimensionless time $t = 10$.

In Figure 1(a) we show decay of the kinetic energy spectrum in the DNS simulation for a combination of parameters that we use throughout the paper: resolution 4096^2 and $Re = 512000$. The spectrum is averaged over 50 realizations of the initial random field. The chosen Reynolds number is very large, and further increase of Re or resolution does not influence significantly the band of scales resolved by the coarse LES models, see squares in Figure 1(b).

Both DNS and LES models are discretized with the same second-order numerical scheme, which is a typical choice in realistic ocean models (Madec et al., 2017; Adcroft et al., 2019). Specifically, we use the Arakawa scheme on the C grid conserving energy and enstrophy (Arakawa, 1997; Maulik & San, 2017c) and second-order approximation of the Poisson equation in (1) which is solved in Fourier space. A three-stage Runge-Kutta (RK3) scheme (Skamarock et al., 2008) is used for time integration, with the time step Δt satisfying the linear stability criterion $CFL = \Delta t \max_j (|u_j|)/\Delta_g < 0.7$, where Δ_g is the grid step.

3 A priori analysis of the interaction with subgrid eddies

In this section, we diagnose the forcing produced by the subgrid eddies on the resolved flow. The analysis of subgrid forcing will guide the development of new subgrid models capable to simulate energy and enstrophy fluxes. We perform the analysis of the subgrid energy budget to propose a parameterization that is energetically consistent, see Jansen and Held (2014). Additionally, we use Germano (1986) decomposition to identify the components of subgrid forcing responsible for the energy and enstrophy fluxes.

3.1 Filtered equations

Following the LES approach (Sagaut, 2006), we introduce a spatial filter $\overline{(\cdot)}$ decomposing the flow into the resolved part and unresolved or subgrid eddies. The filter is Gaussian and defined in Fourier space by the transfer function $\exp(-\overline{\Delta}^2 k^2/24)$, where $\overline{\Delta}$ – filter width. By applying the filter to the governing equations (1), we obtain an equation for the large-scale flow:

$$\frac{\partial \overline{\omega}}{\partial t} + \frac{\partial}{\partial x_j} (\overline{u_j \omega}) = \frac{1}{Re} \nabla^2 \overline{\omega} - \frac{\partial}{\partial x_j} (\sigma_j), \quad \nabla^2 \overline{\psi} = \overline{\omega}, \quad (3)$$

which is unclosed and contains interaction with the subgrid eddies (subgrid flux):

$$\sigma_j = \overline{u_j \omega} - \overline{u_j} \overline{\omega}. \quad (4)$$

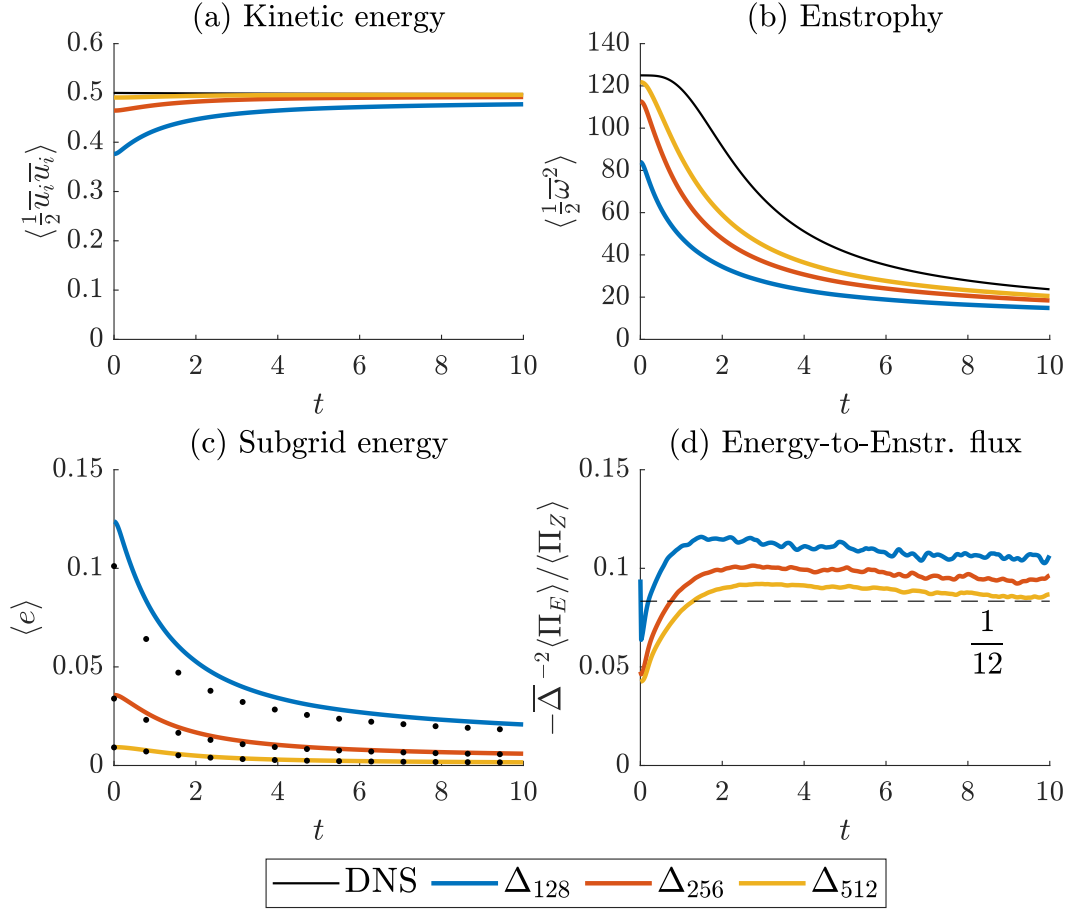


Figure 2. (a) Kinetic energy and (b) enstrophy in DNS (black line) and filtered solutions (in colors), (c) subgrid energy (solid lines) and its estimation according to Eq. (6) in dots, (d) the ratio of energy and enstrophy fluxes; the filter is Gaussian with different widths: $\Delta_{128} > \Delta_{256} > \Delta_{512}$.

The spatial filter mimics the effect of a finite resolution and its width should be proportional to the grid step of the coarse LES model (Δ_g). The Gaussian filters related to the coarse resolutions of 128^2 , 256^2 and 512^2 points are denoted as Δ_{128} , Δ_{256} and Δ_{512} , respectively. We set the filter-to-grid width ratio as $FGR = \overline{\Delta} / \Delta_g = \sqrt{6}$, and explain our choice in Section 5. Note that a priori analysis is performed on a DNS grid, and the coarse model’s grid step is used only to guide the choice of the filter width $\overline{\Delta}$.

3.2 Domain-averaged energy exchange with subgrid eddies

The coarse LES model should simulate the statistical properties of the filtered DNS (Frezat et al., 2022), such as kinetic energy and enstrophy of the filtered solution. The enstrophy of the filtered solution decays (Figure 2(b)), and it is a consequence of the direct enstrophy cascade. On the contrary, the resolved energy in decaying 2D turbulence grows for a very high Reynolds number (Figure 2(a)), and it is a consequence of the redistribution of the kinetic energy towards large scales (inverse cascade, (Kraichnan, 1967; C. E. Leith, 1968; Batchelor, 1969)), see also Figure 9 in Thuburn et al. (2014).

To accurately simulate the energy of the filtered solution, the subgrid parameterization should predict the energy exchange between resolved flow and subgrid eddies. Consider the budget of subgrid kinetic energy (Eq. (7) in Jansen and Held (2014)):

$$\frac{d}{dt}\langle e \rangle = \langle \Pi_E \rangle - \langle D \rangle, \quad (5)$$

where $\langle \cdot \rangle$ is the domain-averaging, $e = \frac{1}{2}(\overline{u_i u_i} - \bar{u}_i \bar{u}_i)$ is the subgrid kinetic energy (Germano, 1992; Ghosal et al., 1995), $D \geq 0$ is the dissipation of subgrid KE, $\Pi_E = \sigma_j \partial_{x_j} \bar{\psi}$ is the energy flux from resolved to subgrid scales. We assume that $D = 0$ because there is no bottom drag in governing equation (Eq. (1)), see Jansen and Held (2014); Jansen et al. (2019). The simplest way to predict the energy flux is to consider a statistically stationary case ($\frac{d}{dt}\langle e \rangle \approx 0$) in equation (5) which gives zero energy exchange between resolved and subgrid scales $\langle \Pi_E \rangle \approx 0$, see Jansen and Held (2014); Thuburn et al. (2014). This approach is not suitable for the simulation of decaying turbulence, which is not stationary. A more accurate approach would include a numerical integration of the equation analogous to (5) as proposed in Jansen et al. (2015). Our diagnostics show that the subgrid kinetic energy decreases ($\frac{d}{dt}\langle e \rangle < 0$, Figure 2(c)), and thus according to Eq. (5) it should contribute to the negative subgrid energy flux, i.e. $\langle \Pi_E \rangle < 0$. That is, subgrid eddies energize the resolved eddies on average. Partee et al. (2022); Khani and Dawson (2023) proposed a new way to predict the energy of subgrid eddies: it can be estimated given the resolved flow as an alternative to the simulation of Eq. (5). The gradient model of Khani and Dawson (2023) predicts the subgrid KE using only the resolved flow as:

$$e = \frac{1}{2} \cdot \frac{\bar{\Delta}^2}{12} \frac{\partial \bar{u}_i}{\partial x_j} \frac{\partial \bar{u}_i}{\partial x_j}, \quad (6)$$

where we used a standard parameter of the gradient model for the Gaussian filter (1/12, Meneveau and Katz (2000)). In Figure 2(c) we show in black dots that the model (Eq. (6)) accurately predicts the diagnosed subgrid KE. Using Eq. (6) and assuming $D = 0$, we can estimate the energy flux $\langle \Pi_E \rangle$ from (5), where d/dt can be approximated with finite differences. Specifically for 2D decaying turbulence, we can further simplify this method to obtain an interpretable relation between energy and enstrophy fluxes (derived in Appendix A):

$$\langle \Pi_E \rangle = -\frac{\bar{\Delta}^2}{12} \langle \Pi_Z \rangle, \quad (7)$$

where $\Pi_Z = -\sigma_j \partial_{x_j} \bar{\omega}$ is the enstrophy flux from resolved to subgrid scales. Forward transfer of enstrophy corresponds to a positive flux $\langle \Pi_Z \rangle > 0$. In Figure 2(d) we show that the diagnosed energy and enstrophy fluxes are directed oppositely on average, and the presented estimate of the energy flux (Eq. (7)) is accurate after the initial adaptation of the turbulence ($t > 1$). The formula (Eq. (7)) will be used to build a new backscatter parameterization.

3.3 Transfer spectra for Germano decomposition

The subgrid energy and enstrophy transfer spectra are given by, respectively (Guan, Subel, et al., 2022):

$$T_E(k) = \sum_{|\mathbf{k}| \in [k, k+1)} \text{Re} \left(\left(\frac{\partial \sigma_j}{\partial x_j} \right)_{\mathbf{k}}^* (\bar{\psi})_{\mathbf{k}} \right), \quad (8)$$

$$T_Z(k) = \sum_{|\mathbf{k}| \in [k, k+1)} \text{Re} \left(- \left(\frac{\partial \sigma_j}{\partial x_j} \right)_{\mathbf{k}}^* (\bar{\omega})_{\mathbf{k}} \right), \quad (9)$$

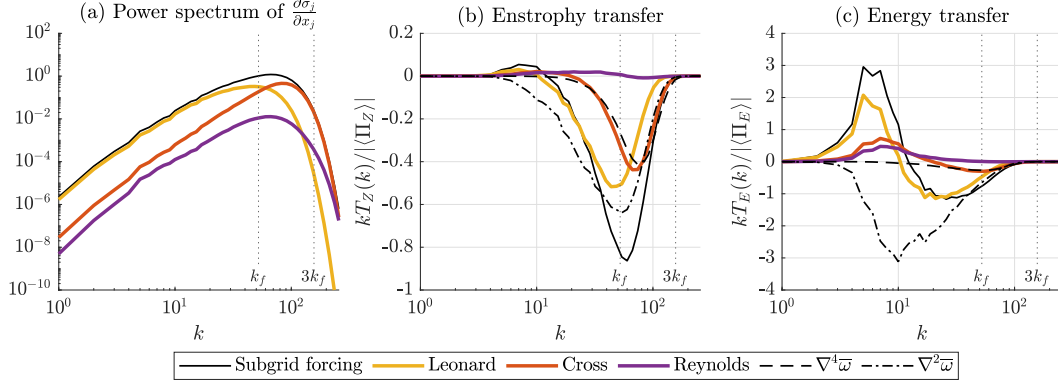


Figure 3. A priori analysis of the subgrid forcing with Germano decomposition (Eq. (11)) for the filter with medium width Δ_{256} , $t = 2$. (a) Power spectrum of subgrid forcing; (b) enstrophy and (c) energy transfer spectra. The filter scale is defined as $k_f = \pi/\bar{\Delta}$; $\nabla^2\bar{\omega}$ and $\nabla^4\bar{\omega}$ are dissipation spectra produced by laplacian and biharmonic eddy viscosity models.

and $(\cdot)_k$ denotes 2D Fourier transform, $(\cdot)^*$ is complex conjugate. These transfer spectra are connected to the energy and enstrophy fluxes (Π_E, Π_Z) as follows:

$$\int T_E(k)dk = -\langle \Pi_E \rangle, \quad \int T_Z(k)dk = -\langle \Pi_Z \rangle. \quad (10)$$

In Figure 3(b,c) we show the transfer spectra in black line. The subgrid energy and enstrophy transfer contains a small-scale dissipative region ($T_E(k) < 0$, $T_Z(k) < 0$) and a large-scale backscatter region ($T_E(k) > 0$, $T_Z(k) > 0$), but the relative contribution of the energy backscatter is higher. We show examples of simple eddy viscosity models (dashed and dot-dashed lines in Figure 3(b,c)). These models are purely dissipative and cannot capture the complex structure of subgrid fluxes.

The Germano (1986) decomposition of subgrid vorticity flux is given by (Nadiga, 2008):

$$\sigma_j = \underbrace{\bar{u}_j \bar{\omega} - \bar{u}_j \bar{\omega}}_{\text{Leonard}} + \underbrace{\bar{u}_j \omega' + \bar{u}'_j \bar{\omega} - \bar{u}_j \bar{\omega}' - \bar{u}'_j \bar{\omega}}_{\text{Cross}} + \underbrace{\bar{u}'_j \omega' - \bar{u}'_j \bar{\omega}'}_{\text{Reynolds}}, \quad (11)$$

where primed quantities denote subgrid eddies, $\omega' = \omega - \bar{\omega}$ and $u'_j = u_j - \bar{u}_j$. The Reynolds stress represents the effect on the resolved flow from eddy-eddy interactions, Cross stress represents the effect of eddy-resolved flow interactions. Finally, the Leonard stress contains only the resolved fields and can be directly computed given \bar{u}_j and $\bar{\omega}$.

In Figure 3 we show the spectral content for each component in the Germano decomposition. The enstrophy dissipation is mostly represented by Leonard and Cross stresses, see Figure 3(b). Also, the enstrophy dissipation by the Cross stress can be approximated by the biharmonic viscosity model ($\nabla^4\bar{\omega}$), see the dashed line in Figure 3(b). These findings will be used to propose a mixed dissipative model of subgrid forcing. The kinetic energy backscatter is influenced by Leonard, Cross and Reynolds stresses, but only the Reynolds stress almost purely represents the positive energy transfer (Figure 3(c)), and this property will be used to propose a new backscatter model. The contribution of Germano decomposition components to the energy and enstrophy transfer is similar for the other filter widths.

4 Subgrid models

In this section, we describe the dynamic Smagorinsky model and propose new dissipative and backscattering models by applying the results of a priori analysis.

4.1 Dynamic Smagorinsky model (DSM)

The dynamic Smagorinsky model (DSM) is a popular baseline subgrid model in quasi-2D turbulence research (Maulik & San, 2017b; Pawar et al., 2020; Guan, Chattopadhyay, et al., 2022; Frezat et al., 2022). The Smagorinsky eddy viscosity model is given by:

$$\sigma_j \approx \sigma_j^{DSM} = -C_S^2 \bar{\Delta}^2 |\bar{S}| \frac{\partial \bar{\omega}}{\partial x_j}, \quad (12)$$

where C_S is the Smagorinsky coefficient. Filtered strain-rate tensor is $\bar{S}_{ij} = \frac{1}{2} (\partial_{x_j} \bar{u}_i + \partial_{x_i} \bar{u}_j)$ and its modulus $|\bar{S}| = \sqrt{2\bar{S}_{ij}\bar{S}_{ij}}$. In the dynamic model of Germano et al. (1991), a free parameter (C_S) is estimated from the resolved subgrid flux $l_j = \widehat{u_j \bar{\omega}} - \widehat{u_j} \widehat{\bar{\omega}}$, where a new test filter $\widehat{(\cdot)}$ of width $\widehat{\Delta}$ is introduced. The resolved subgrid flux can be decomposed as follows (Germano identity):

$$l_j = \Sigma_j - \widehat{\sigma}_j, \quad (13)$$

where $\Sigma_j = \widehat{u_j \bar{\omega}} - \widehat{u_j} \widehat{\bar{\omega}}$ is the subgrid flux with respect to the combined filter $\widehat{(\cdot)}$ of width $\widehat{\Delta} = \sqrt{\bar{\Delta}^2 + \widehat{\Delta}^2}$ (Germano, 1992). Substituting Smagorinsky model (12) to the Germano identity (13) and applying least squares procedure of Ghosal et al. (1995), we determine the Smagorinsky coefficient:

$$C_S^2 = \frac{\langle l_j \alpha_j \rangle}{\langle \alpha_j \alpha_j \rangle}, \quad (14)$$

where $\langle \cdot \rangle$ is the spatial averaging and

$$\alpha_j = -\widehat{\Delta}^2 |\widehat{S}| \frac{\partial \widehat{\bar{\omega}}}{\partial x_j} + \overline{\bar{\Delta}^2 |\bar{S}| \frac{\partial \bar{\omega}}{\partial x_j}}. \quad (15)$$

To reduce the number of free parameters, we set the test filter equal to the base filter, i.e. $\widehat{(\cdot)} = \overline{(\cdot)}$, and consequently $\widehat{\Delta}/\bar{\Delta} = \sqrt{2}$.

The spectral properties of the DSM model (Eq. (12) and (14)) in a priori analysis are shown in Figure 4. The DSM is a purely dissipative model, and it predicts the enstrophy dissipation of the subgrid forcing reasonably well (Figure 4(b)). However, it introduces the dissipation of kinetic energy on large scales, where the subgrid forcing has a significant positive transfer, i.e. backscatter (Figure 4(c)). Thus we conclude that DSM model is inconsistent with the physics of the quasi-2D fluids, and it needs to be modified.

4.2 Dynamic mixed model (DMM)

We first leverage the approach of mixed models (Meneveau & Katz, 2000) to model the dissipation of enstrophy. The classical mixed model combines Leonard stress (also known as the scale-similarity model, SSM, Bardina et al. (1980)) with the laplacian Smagorinsky eddy viscosity model (Guan, Subel, et al., 2022). However, we have shown in a priori analysis that the enstrophy dissipation is accurately represented by the combination of the Leonard stress with biharmonic eddy viscosity. We utilize this finding in the mixed model as follows:

$$\sigma_j^{DMM} = \overline{u_j \bar{\omega}} - \overline{u_j} \overline{\bar{\omega}} + C_S^4 \bar{\Delta}^4 |\bar{S}| \frac{\partial(\nabla^2 \bar{\omega})}{\partial x_j}, \quad (16)$$

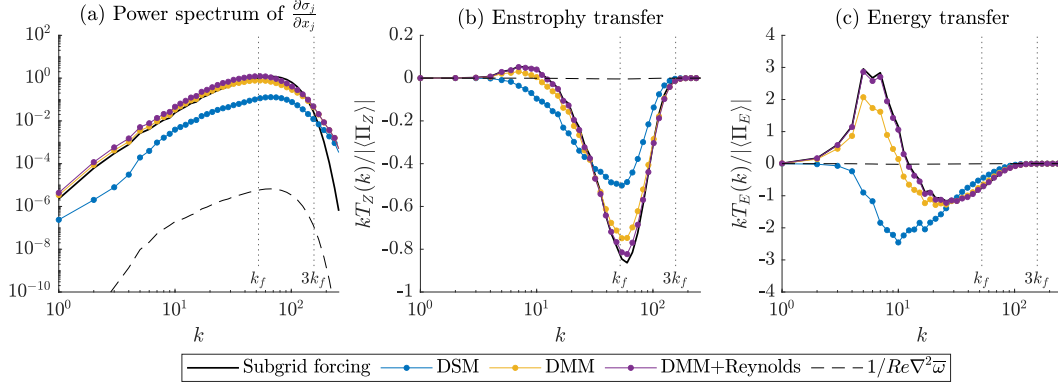


Figure 4. A priori analysis of subgrid models: DSM is dynamic Smagorinsky model, DMM is dynamic mixed model comprising Leonard stress, DMM+Reynolds includes an additional backscatter parameterization (Reynolds stress). Medium filter width Δ_{256} and $t = 2$. Subgrid models are computed given the filtered DNS data on the grid of DNS. Dashed line shows contribution of the molecular viscosity at $Re = 512000$.

and dynamic procedure to determine the Smagorinsky coefficient:

$$C_S^4 = \frac{\langle (l_j - h_j) \alpha_j \rangle}{\langle \alpha_j \alpha_j \rangle}, \quad (17)$$

where

$$\alpha_j = \widehat{\Delta}^4 |\widehat{S}| \frac{\partial \nabla^2 \widehat{\omega}}{\partial x_j} - \overline{\widehat{\Delta}^4 |\widehat{S}| \frac{\partial \nabla^2 \overline{\omega}}{\partial x_j}} \text{ and } h_j = \widehat{\widehat{u_j \overline{\omega}}} - \widehat{\widehat{u_j}} \widehat{\overline{\omega}} - \left(\widehat{\widehat{u_j \overline{\omega}}} - \widehat{\widehat{u_j}} \widehat{\overline{\omega}} \right), \quad (18)$$

see also Vreman et al. (1994) for definition of h_j .

The a priori analysis with the DMM model (Eq. (16) and (17)) shows an improvement in the enstrophy dissipation spectrum, power spectrum and kinetic energy backscattering in large scales, see Figure 4. However, the positive energy transfer on large scales by the DMM model is clearly underestimated, and it needs to be further modified to account for the missing backscatter.

4.3 DMM with backscattering part (DMM+Reynolds)

We have shown in a priori analysis that the Reynolds stress is a promising candidate for an additional backscatter model: it has a small contribution to the enstrophy budget and almost purely represents a positive transfer of kinetic energy. The Reynolds stress cannot be computed given the filtered fields $\overline{\omega}$ and $\overline{u_j}$, but can be approximated as follows:

$$\overline{u'_j \omega'} - \overline{u'_j} \overline{\omega'} \approx \sigma_j^{KEB} = \overline{\overline{u'_j \omega'}} - \overline{\overline{u'_j}} \overline{\overline{\omega'}}, \quad (19)$$

where $\overline{u'_j} = \overline{u_j} - \overline{\overline{u_j}}$ and $\overline{\omega'} = \overline{\omega} - \overline{\overline{\omega}}$, see Horiuti (1997) for details. The modification to DMM model accounting for an additional backscatter then reads:

$$\sigma_j = \sigma_j^{DMM} + C_R \sigma_j^{KEB}, \quad (20)$$

where σ_j^{DMM} and its parameter C_S are set in the previous section. The energy balance equation (7) reads as $\langle \sigma_j \partial_{x_j} \overline{\psi} \rangle = \frac{\overline{\Delta}^2}{12} \langle \sigma_j \partial_{x_j} \overline{\omega} \rangle$, and allows to choose a free parameter C_R as follows:

$$C_R = - \frac{\langle \sigma_j^{DMM} \beta_j \rangle}{\langle \sigma_j^{KEB} \beta_j \rangle}, \quad (21)$$

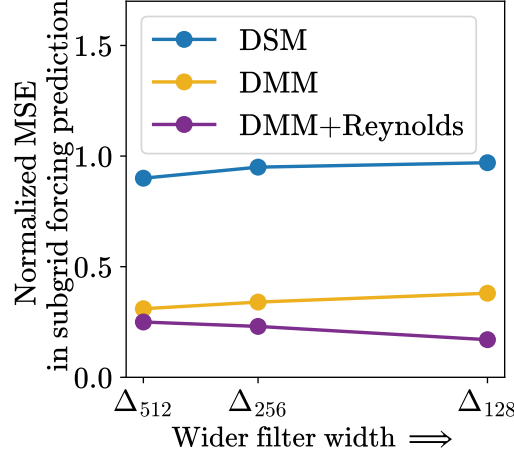


Figure 5. Mean squared error (MSE) in a priori analysis of subgrid models on DNS grid, averaged over $t \in [2, 10]$. Error at a single time is: $\text{MSE} = \langle (\partial_{x_j} \sigma_j - \partial_{x_j} \sigma_j^m)^2 \rangle / \langle (\partial_{x_j} \sigma_j)^2 \rangle$, where σ_j is the subgrid flux and σ_j^m is a subgrid model.

where

$$\beta_j = \frac{\partial \bar{\psi}}{\partial x_j} - \frac{\bar{\Delta}^2}{12} \frac{\partial \bar{\omega}}{\partial x_j}. \quad (22)$$

The proposed DMM+Reynolds model (Eq. (20) and (21)) demonstrates excellent a priori results: it is same good as the DMM model in reproducing the power spectrum and enstrophy dissipation (Figure 4(a,b)), but additionally improves kinetic energy backscatter on large scales (Figure 4(c)).

The proposed modifications to the dynamic Smagorinsky model (DMM and DMM+Reynolds) significantly improve the MSE error in the prediction of subgrid forcing, see Figure 5. We emphasize that the improvement due to including the parameterization of Reynolds stress increases as the filter gets wider, which is expectable because subgrid and Reynolds stresses should be equal for a very large filter width (Sullivan et al., 2003).

4.4 Numerical discretization of subgrid models

We discretize the subgrid models (DSM, DMM and DMM+Reynolds) with the second-order numerical schemes. The spatial Gaussian filter is implemented in Fourier space if $\epsilon = \bar{\Delta}/\Delta_g > \sqrt{6}$ and using second-order approximation otherwise (Sagaut & Grohens, 1999):

$$\bar{\phi} = \frac{1}{24} \epsilon^2 (\phi_{j+1} + \phi_{j-1}) + (1 - \frac{\epsilon^2}{12}) \phi_j, \quad (23)$$

where j is an index of a grid node in one direction. The two-dimensional discrete filter is given by a sequential application of one-dimensional filters (23) along x_1 and x_2 , i.e. filter product, see Sagaut and Grohens (1999). A combination of filters $\widehat{(\cdot)}$ is given by a sequential application of the base and test filters. The only tunable parameter remains in the coarse LES models: filter-to-grid width ratio $\bar{\Delta}/\Delta_g$, and we discuss it in the next section.

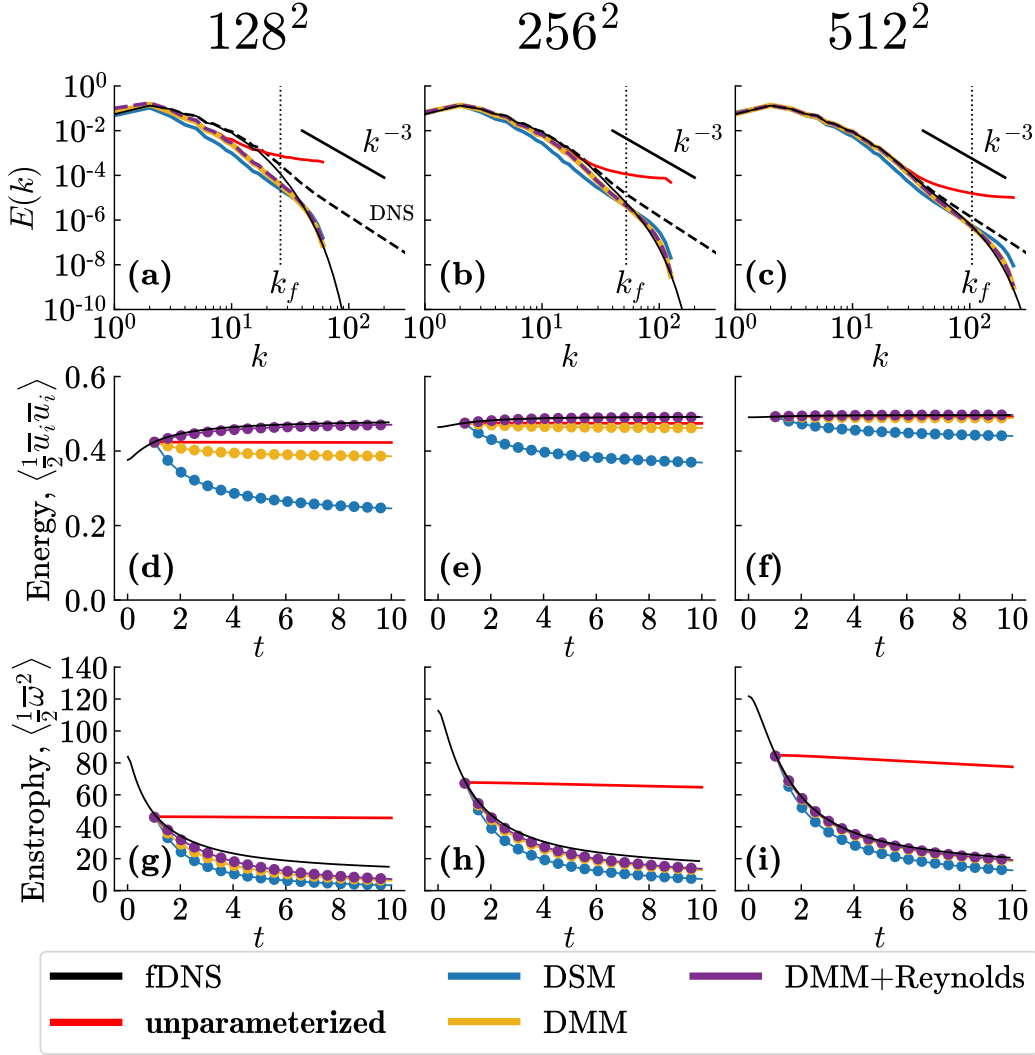


Figure 6. A posteriori experiments with subgrid models integrated with zero viscosity ($\frac{1}{Re}\nabla^2\bar{\omega} = 0$); unparameterized simulation ($\sigma_j = 0$) shows the dissipation introduced by the time integration scheme. Upper row: spectrum of KE at $t = 10$, middle row: kinetic energy, bottom row: enstrophy. DNS at resolution 4096^2 and $Re = 512000$ is used as a reference solution.

5 A posteriori experiments

In this section, we implement the proposed subgrid models into the LES equation (3), and perform a posteriori experiments. The goal for LES models is to reproduce filtered DNS (fDNS) data on a coarse grid.

5.1 Comparison of subgrid models

As a reference solution, we use DNS at resolution 4096^2 and $Re = 512000$. In order to demonstrate that the proposed subgrid models do not generate numerical noise, we integrate LES equation (3) on a coarse grid without molecular viscosity ($\frac{1}{Re}\nabla^2\bar{\omega} = 0$). Note that results with molecular viscosity are almost identical. We also provide simulations with unparameterized model ($\sigma_j = 0$), where the only dissipation

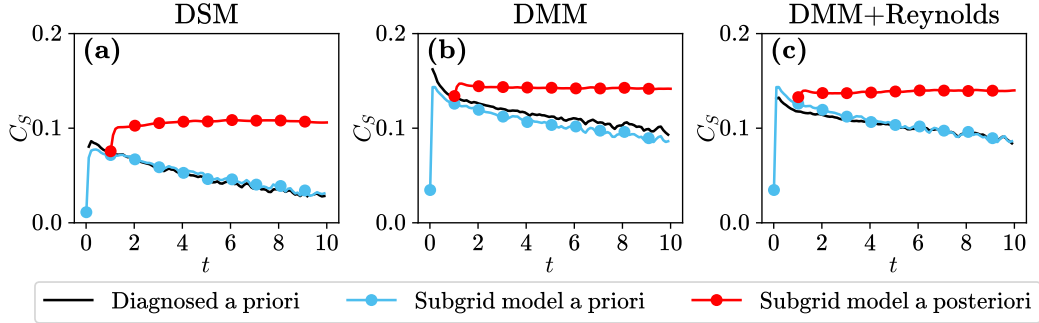


Figure 7. Comparison of the predicted and diagnosed Smagorinsky coefficient (C_S). Black line: C_S diagnosed from DNS data, blue line: prediction of C_S by dynamic model on filtered DNS data, red line: prediction by dynamic model in a posteriori experiment. All experiments have $Re = 512000$ and filter width Δ_{128} .

is related to the time integration scheme (RK3). Neglecting molecular viscosity is a common practice in realistic ocean models, and in our case it is justified by its low impact on scales of the coarse LES models, see Figures 1 and 4.

Every experiment is computed for an ensemble of 50 realizations. Numerical integration starts at $t = 1$, and the initial condition is prepared from DNS data as follows. We first apply a Gaussian filter of width $\bar{\Delta}$ to DNS fields, and then perform spectral truncation of wavenumbers $|k_i| > \pi/\Delta_g$, where Δ_g is the grid step of a coarse LES model. We run a posteriori experiments for three resolutions (128^2 , 256^2 , 512^2) at a fixed FGR: $\bar{\Delta}/\Delta_g = \sqrt{6}$. This parameter was chosen based on the sensitivity studies and corresponds to a tradeoff between the strength of discretization errors and the number of directly resolved turbulent eddies, see Appendix B.

All the proposed dynamic models (DSM, DMM, DMM+Reynolds) produce numerically stable solutions without build-up of energy spectrum near the grid scale for a range of resolutions, see upper row in Figure 6. The mixed models (DMM and DMM+Reynolds) are superior to the baseline DSM. They better reproduce the shape of the energy spectrum of fDNS near the filter scale (k_f) and in middle scales, see Figure 6(a,b,c). The DSM model dissipates too much energy, and DMM model allows to reduce the dissipation. The inclusion of the Reynolds stress introduces the kinetic energy backscatter which allows to simulate the growth of the kinetic energy (Figure 6(d,e,f)). Note that the effect of the Reynolds stress is enlarging for coarser resolutions consistently with a priori analysis. The decay of enstrophy is improved with the use of new mixed models compared to the baseline DSM (Figure 6(g,h,i)).

5.2 Scale invariance

The scale similarity of the kinetic energy spectrum in DNS breaks at the largest scales when ever-enlarging eddies condensate and result in a spectrum different from the power law. Once the eddy scale falls within the subgrid range, all subgrid models fail to reproduce the complicated shape of fDNS spectrum and predict a power law, see Figure 6(a). For example, the subgrid model DMM+Reynolds energizes the flow, but additional energy resides in the largest scales almost without improving the middle ones compared to DMM. An excessive dissipation of enstrophy (Figure 6(g)) also indicates that the middle scales are too damped. In this section, we investigate the influence of the scale invariance on the performance of subgrid models.

Dynamic subgrid models are built on the assumption that the Smagorinsky coefficient is scale-invariant, i.e. it is independent of the filter width. However, this assumption violates whenever we deal with a break of self-similarity of the energy spectrum. For this case, a scale-dependent dynamic model was proposed (Meneveau & Lund, 1997; Porté-Agel et al., 2000). Likewise, the scale invariance of the Smagorinsky model can be violated for quasi-2D flows exhibiting the enstrophy cascade, and for this case C. Leith (1996) proposed a new eddy viscosity model (Fox-Kemper & Menemenlis, 2008; Bachman et al., 2017). A break of the scale invariance of the Smagorinsky model can potentially lead to an inaccurate prediction of the Smagorinsky coefficient by the dynamic procedure of Germano et al. (1991).

In Figure 7(a), we show in black line the Smagorinsky coefficient (C_S) diagnosed from the DNS data by the least squares fit of the subgrid flux σ_j :

$$C_S^2 = \frac{\langle \sigma_j \alpha_j \rangle}{\langle \alpha_j \alpha_j \rangle}, \quad \alpha_j = -\bar{\Delta}^2 |\bar{S}| \frac{\partial \bar{\omega}}{\partial x_j}. \quad (24)$$

The subgrid model DSM applied to filtered DNS data (Eq. (14)) accurately predicts the diagnosed parameter C_S , see blue line in Figure 7(a). However, once we evaluate the subgrid model a posteriori, the Smagorinsky coefficient abruptly increases (red line in Figure 7(a)) and it results in the excessive dissipation of enstrophy. We conclude that the scale invariance of the eddy viscosity model has a minor effect on the accuracy of the dynamic procedure, but the main difficulty is in the lack of consistency between a priori and a posteriori performance of the same subgrid model (Ross et al., 2023).

In Figure 7(b,c) we show similar difference between a priori and a posteriori results for DMM and DMM+Reynolds models. Note that diagnosed C_S is slightly different for these models, because the least squares fit for DMM+Reynolds model includes additional parameter C_R . The diagnosed and predicted values of this parameter are close to $C_R \approx 20$, and we do not show it.

6 Implementation to QG and primitive equation ocean models

We suggest that a similar analysis should be performed in a more realistic set of equations before dynamic mixed parameterizations can be successfully used in ocean simulations. An important outcome of our study is to show that the Reynolds stress can be used as a backscatter parameterization. This is demonstrated in this section in experiments in quasi-geostrophic (QG) and primitive equation ocean models.

6.1 Two-layer QG model

We use an idealized QG ocean model (pyqg, Abernathey et al. (2022)). Our configuration is called "eddy" and described in Ross et al. (2023); P. Perezhugin et al. (2023). The model has two fluid layers in a doubly-periodic domain. It is forced by the prescribed vertical shear of a zonal flow and loses its energy by frictional dissipation in the bottom layer. The numerical scheme is pseudospectral with a highly scale-selective dissipation, which removes enstrophy and numerical noise near the grid scale.

We extend the Reynolds model (Eq. (19)) to simulate the subgrid flux of potential vorticity (PV) as follows:

$$\frac{\partial q}{\partial t} = \dots - C_R \frac{\partial}{\partial x_j} \left(\overline{u'_j q'} - \overline{u'_j} \overline{q'} \right), \quad (25)$$

where q and u_j are the resolved PV and velocity on a coarse grid; $q' = q - \bar{q}$ and $u'_j = u_j - \bar{u}_j$. Note that we omitted one filtering operation in (25) for clarity of numerical implementation (see Section 1.3 in Layton and Rebholz (2012)). The filter (\cdot) is Gaussian with $\bar{\Delta}/\Delta_g = 2$. The parameterization is applied layerwise with the

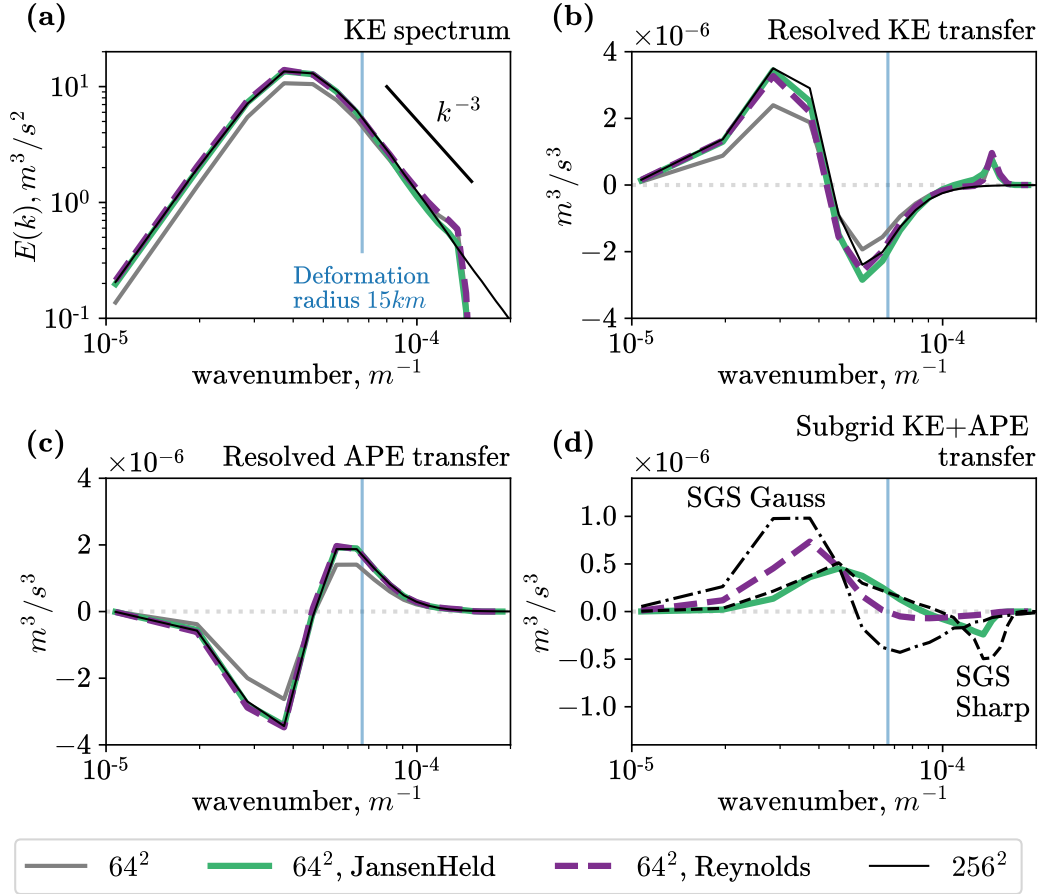


Figure 8. Experiments in two-layer QG idealized ocean model. High-resolution simulation (256^2) is compared to models at coarse resolution, where 64^2 denotes unparameterized simulation, JansenHeld denotes negative viscosity backscatter, and Reynolds is given in Eq. (25). (a) Kinetic energy spectrum, (b) resolved transfer of KE, (c) resolved transfer of APE, (d) transfer of total energy by subgrid parameterizations.

same C_R which controls the strength of energy injection. We found an optimal value $C_R = 7$ by matching the KE spectrum on large scales for high-resolution and coarse parameterized models.

We choose the parameterization of Jansen and Held (2014); Jansen et al. (2015) as a baseline subgrid model. Implementation details are provided in Ross et al. (2023), and we choose the optimal parameters of the parameterization from this paper. Jansen-Held subgrid model consists of two parts: small-scale dissipation parameterized by biharmonic viscosity and larger-scale backscatter parameterized by laplacian operator with negative viscosity.

In Figure 8 we compare coarse models on a grid 64^2 (grid step 15.6km) to the high-resolution simulation (256^2 , 3.9km) after reaching statistical equilibrium: we average the results between 5 and 20 years of the simulation for an ensemble of 10 members. The energy cycle comprises two cascades (Salmon, 1978; Vallis, 2017). The available potential energy (APE) is redistributed towards smaller scales following the direct cascade (Figure 8(c)), where it is converted to the kinetic energy near the Rossby deformation radius. The kinetic energy is redistributed towards larger scales following the inverse cascade (Figure 8(b)). The coarse model fails to simulate the energy transfer, and its KE spectral density is smaller compared to the high-resolution model (Figure 8(a)). Both backscatter parameterizations (Reynolds and JansenHeld) simulate the energy injection in the large scales (Figure 8(d)) and amplify the resolved (i.e., unparameterized) cascades of KE and APE (Figure 8(b,c)), which results in a significant improvement in the reproducing of the kinetic energy spectrum. We note that the Reynolds parameterization almost does not change the shape of the KE spectrum near the grid scale and predominantly affects the largest scales. In Figure 8(d) we compare subgrid models in a posteriori experiments to the subgrid forcing diagnosed a priori, see P. Perezhogin et al. (2023). The negative viscosity parameterization (JansenHeld) is suitable for the Sharp filter (see Kraichnan (1976) for explanation), and the Reynolds parameterization is closer to the subgrid forcing diagnosed with the Gaussian filter.

6.2 Primitive equation ocean model NEMO

We use the primitive equation ocean model NEMO (Madec et al., 2017) in the Double Gyre configuration (Lévy et al., 2010). The model contains 30 vertical layers in a domain with a flat bottom and vertical walls. The circulation is forced by the prescribed wind stress and buoyancy fluxes on the surface; the equation of state is linear and comprises temperature and salinity. The coarse and reference models have the resolutions of $1/4^\circ$ (grid step 26.5km) and $1/9^\circ$ (11.7km), respectively. The coarse model starts from the snapshot of the high-resolution model, spin-up for 10 years, and integrated for 20 more years to collect statistics. The small-scale dissipation is given by the biharmonic viscosity with a constant coefficient unique for each resolution, see P. A. Perezhogin (2020) for model parameters. We use a similar baseline subgrid model as in QG simulation: an analog of Jansen and Held (2014) backscatter parameterization implemented by the author (P. Perezhogin, 2019; P. A. Perezhogin, 2020). We use the optimal parameters of the parameterization from these papers.

We extend the Reynolds parameterization (Eq. (19)) to simulate the subgrid momentum flux as follows:

$$\frac{\partial u_i}{\partial t} = \dots - \frac{\partial}{\partial x_j} \left(C_R \left(u'_i u'_j - \overline{u'_i u'_j} \right) \right), \quad i, j \in \{1, 2\}, \quad (26)$$

where u_i is the resolved horizontal velocity on a coarse grid and $u'_i = u_i - \overline{u_i}$. The parameterization is applied layerwise with the same C_R . We observed that if C_R is tuned to improve the kinetic energy, the wider filter (\cdot) allows choosing the lower parameter

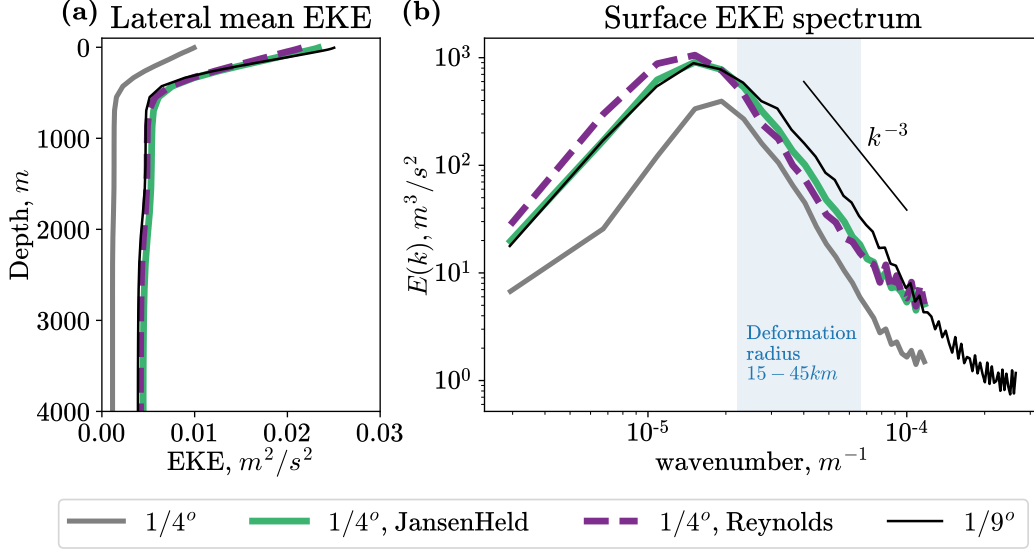


Figure 9. Experiments in NEMO ocean model in Double Gyre configuration. (a) 20-year mean eddy kinetic energy averaged laterally over the whole domain. (b) spatial spectrum of surface eddy kinetic energy (half the power spectrum of velocity deviations from 1-year mean flow).

RMSE	SSH, m	SST, $^\circ C$	SSS, psu
$1/4^\circ$	0.108	0.647	0.128
$1/4^\circ$, JansenHeld	0.06 (-44.16%)	0.404 (-37.6%)	0.112 (-12.53%)
$1/4^\circ$, Reynolds	0.061 (-43.64%)	0.321 (-50.38%)	0.081 (-36.38%)

Table 1. The root mean squared errors (RMSE) in 20-year mean sea surface height (SSH), sea surface temperature (SST) and sea surface salinity (SSS). The error is computed w.r.t. $1/9^\circ$ model.

C_R . Consequently, we define the filter $\overline{(\cdot)}$ as 2 iterations of the 3-point filter (Eq. (23)) with maximum allowable $\epsilon = \sqrt{6}$. The 3-point filter imposes physical boundary conditions on the velocity: no-normal flow and free slip. To avoid setting boundary conditions on momentum flux, we assume commutation of filter and derivative and compute the first part of the parameterization as follows: $\frac{\partial}{\partial x_j} \left(C_R \overline{u'_i u'_j} \right) \rightarrow \frac{\partial}{\partial x_j} \left(C_R u'_i u'_j \right)$. In preliminary experiments, we realized that it is important to reduce the influence of the boundaries. Therefore, we attenuate the strength of the parameterization smoothly in the vicinity of the wall ($l \leq L$) as follows: $C_R \rightarrow C_R \cdot (1 - \cos(\pi l/L))/2$, where l is the distance to the wall and L is the length scale of attenuation. After some tuning, we set L as 4 grid steps. The only free parameter $C_R = 30$ was chosen from energetic considerations: to obtain the best RMSE in the vertical profile of eddy kinetic energy (EKE).

The Reynolds model works as a backscatter parameterization and energizes the flow on a coarse grid. Similarly to the JansenHeld subgrid model, the EKE can be increased near the surface and the bottom, see Figure 9(a). The spectrum of EKE indicates an increase of energy density in all resolved scales for both backscatter parameterizations, see Figure 9(b). An improvement in the representation of the resolved

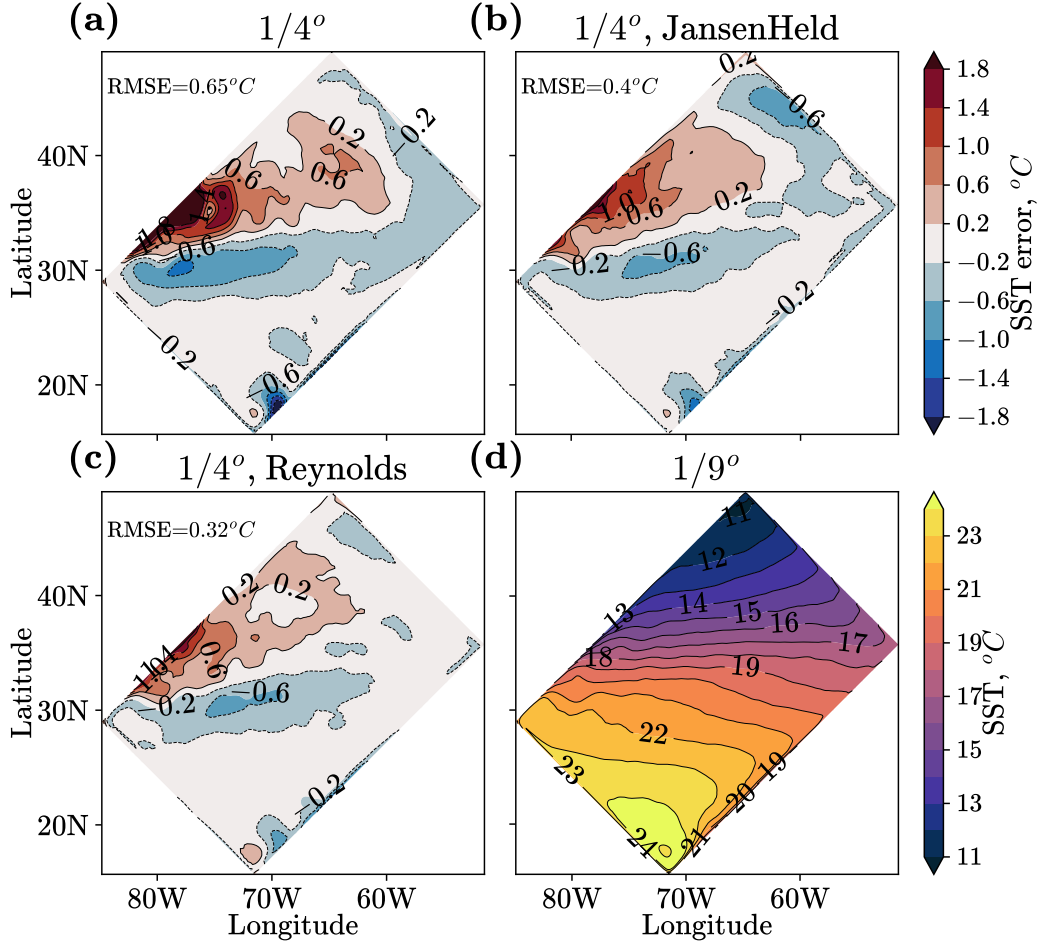


Figure 10. Experiments in NEMO ocean model. (d) 20-year mean sea surface temperature (SST) in the high-resolution model; (a), (b), (c) errors in SST for coarse models. The Reynolds-parameterized model in panel (c) is given in Eq. (26).

eddy activity results in an improvement in several other metrics. In Figure 10 we show 20-year mean sea surface temperature (SST) for the reference simulation and errors for coarse models. The largest error for the unparameterized model is concentrated near the western boundary (Figure 10(a)) and is explained by the misrepresentation of the western boundary current (WBC, Lévy et al. (2010)). Both backscatter parameterizations improve the mean SST near the western boundary (Figure 10(b,c)), but the Reynolds model is also better in the northern region (Figure 10(c)). The RMSE in surface fields for temperature and salinity indicates lower errors for the Reynolds model, see Table 1. In Figure 11 we show 20-year mean meridional overturning circulation (MOC) streamfunction (Cabanès et al., 2008). Both backscatter parameterizations improve the streamfunction near the latitude of WBC separation ($\sim 30^\circ N$), but Reynolds parameterization is also better in improving the northern circulation cell ($\sim 45^\circ N$). Additionally, we show that both backscatter parameterizations significantly improve the resolved eddy meridional heat flux near the latitude $\sim 30^\circ N$ (see Figure 11).

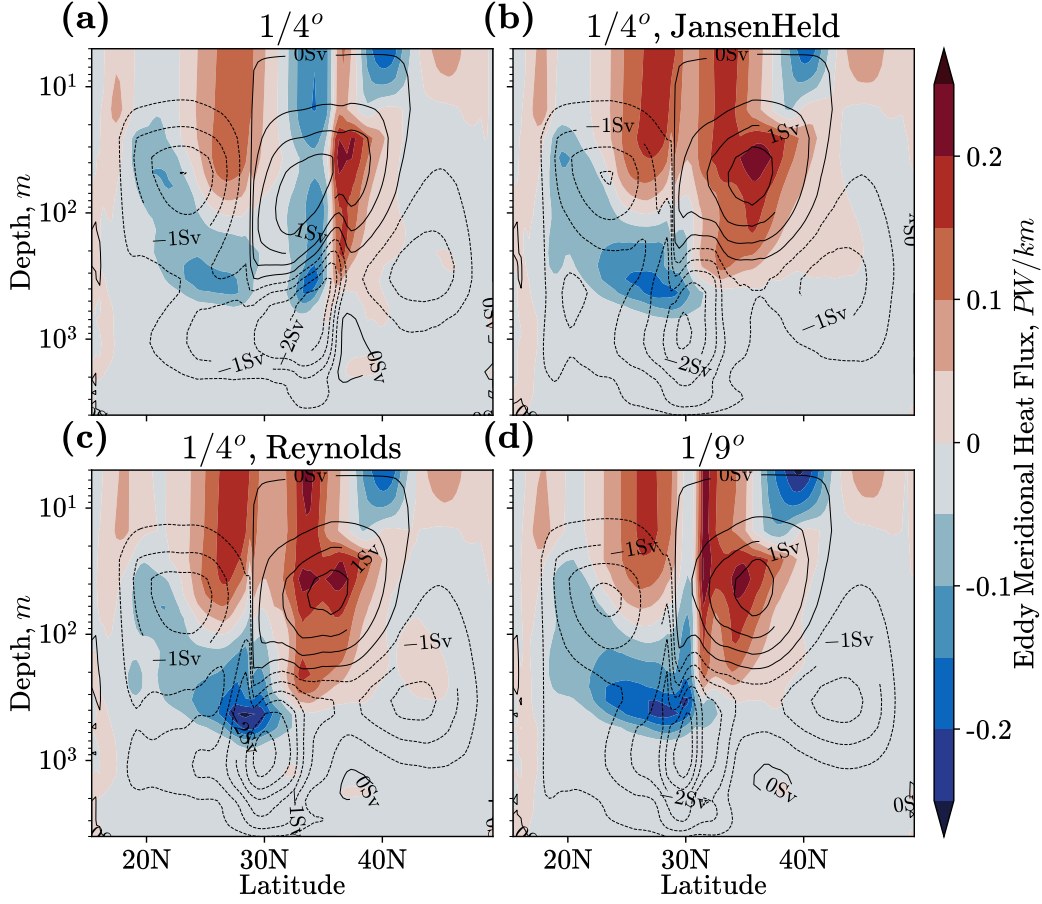


Figure 11. Experiments in NEMO ocean model. In contours: MOC streamfunction computed as $\Psi_{MOC} = \int_{-H}^z \int_{\text{west}}^{\text{east}} \langle V \rangle_t dx dz$ in Sverdrups, where $\langle V \rangle_t$ – 20-year mean meridional velocity. In color: the resolved meridional eddy heat flux, defined as zonal integral of $\rho_0 C_p (\langle TV \rangle_t - \langle T \rangle_t \langle V \rangle_t)$, see P. A. Perezhgin (2020).

7 Conclusions

In this work, we perform careful a priori analysis of energy and enstrophy fluxes in 2D decaying turbulence and develop mixed subgrid parameterizations based on previous studies (Germano, 1986; Germano et al., 1991; Vreman et al., 1994; Horiuti, 1997), but in the context of 2D fluids. We evaluate these parameterizations in a posteriori experiments for a range of resolutions and implement the Reynolds part of the new parameterization to quasi-geostrophic and primitive equation ocean models.

Our main contributions and findings are as follows:

- We consider the budget of subgrid KE (Jansen & Held, 2014) and estimation of subgrid KE (Khani & Dawson, 2023) to predict the domain-averaged kinetic energy flux produced by subgrid eddies, which is required to propose backscatter parameterization.
- The components of Germano decomposition play a special role in forming energy and enstrophy subgrid fluxes: Leonard and Cross stresses are responsible for the enstrophy dissipation; all three stresses (Leonard, Cross, Reynolds) contribute to the kinetic energy backscatter in large scales, but only the Reynolds stress produces almost positive-definite kinetic energy transfer.
- We start from the dynamic Smagorinsky model (DSM) in a priori analysis and show by gradual changes how to build a subgrid model which correctly simulates energy and enstrophy fluxes. In particular, we simulate the enstrophy dissipation by the Leonard stress and the biharmonic Smagorinsky model which approximates the Cross stress; an approximation to the Reynolds stress is used to simulate a missing backscatter of kinetic energy.
- The new subgrid parameterization (DMM+Reynolds) is numerically stable at zero molecular viscosity. It improves the reproduction of the kinetic energy spectrum and decay of enstrophy. The new method to estimate the subgrid energy flux allows to reproduce the growth of the resolved kinetic energy at a very high Reynolds number.
- The role of the Reynolds stress model as a kinetic energy backscatter parameterization holds in two additional ocean models: pseudospectral QG model and finite volume primitive equation model NEMO. Similarly to the Jansen and Held (2014) backscatter parameterization, the Reynolds model allows to energize the flow and improves various statistical properties, such as KE spectrum, the vertical profile of EKE, interscale KE and APE transfers, the resolved meridional eddy heat flux, MOC and errors in surface fields, such as SST, SSS and SSH.

The important result of our analysis is that our subgrid parameterizations do not contain free physical parameters. The only parameter that was tuned a posteriori is the filter-to-grid width ratio (FGR) which was shown to control the relative importance of the numerical discretization errors. We expect that the dynamic procedure to determine the Smagorinsky coefficient (C_S) can be extended to more complex governing equations. Various approaches can be proposed to choose backscattering coefficient (C_R): the procedure here suggested (Eqs. (5) and (6)) can be extended with realistic sinks and sources of subgrid KE (Jansen et al., 2019); C_R can be determined dynamically (Horiuti, 1997; Yuan et al., 2020) or can be used as a tunable parameter. Importantly, C_R can be easily tuned manually, and in our experiments with the NEMO ocean model we showed it can be chosen uniquely for all depths and spatial locations.

Additional future studies related to Germano decomposition can allow us to gain new insights on subgrid modeling. For example, we have shown that the role of the Reynolds stress model increases as the filter gets wider, as it is seen in the a priori MSE metric, simulation of resolved kinetic energy a posteriori, and better results in the

northern region in NEMO ocean model, where Rossby deformation radius falls within subgrid scales. Consequently, new subgrid parameterizations for coarse models can be based on the prediction of the Reynolds stress instead of the full subgrid forcing, see for example, in the context of machine learning (Bolton & Zanna, 2019; Zanna & Bolton, 2020). We demonstrated that the most severe discrepancy between predicted and diagnosed Smagorinsky coefficient comes not from the lack of scale invariance, but from a difference between a priori and a posteriori performance of the same dynamic model. We suggest that the crudest approximation in our DMM+Reynolds model comes from the representation of the Cross stress. New accurate models of the Cross stress could potentially improve the consistency of a priori and a posteriori experiments, and gain a posteriori performance.

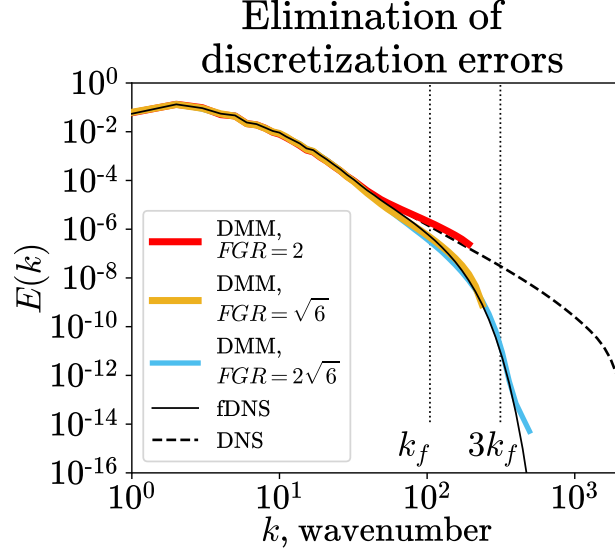


Figure B1. Eliminating discretization errors in a posteriori experiments by enlarging the $FGR = \bar{\Delta}/\Delta_g$ parameter, where filter width is fixed ($\bar{\Delta} = \Delta_{512}$) and grid step is varying; $t = 10$. Experiments with FGR equal to 2, $\sqrt{6}$ and $2\sqrt{6}$ have resolutions 418^2 , 512^2 , 1024^2 , respectively.

Appendix A Estimation of subgrid energy flux

We decompose velocity gradient tensor $\frac{\partial \bar{u}_i}{\partial x_j}$ into symmetric \bar{S}_{ij} and antisymmetric $\bar{\Omega}_{ij}$ parts, and consequently $\frac{\partial \bar{u}_i}{\partial x_j} \frac{\partial \bar{u}_i}{\partial x_j} = \bar{S}_{ij} \bar{S}_{ij} + \bar{\Omega}_{ij} \bar{\Omega}_{ij} = |\bar{S}|^2/2 + \bar{\omega}^2/2$ (Borue & Orszag, 1998). On a periodic domain, we have $\langle |\bar{S}|^2 \rangle = \langle \bar{\omega}^2 \rangle$ (Buxton et al., 2011). Finally, the estimation of subgrid KE (Eq. (6)) is related to the resolved enstrophy ($Z = \bar{\omega}^2/2$) as:

$$\langle e \rangle = \frac{\bar{\Delta}^2}{12} \langle Z \rangle. \quad (\text{A1})$$

At a high Reynolds number, the resolved enstrophy can be lost only to the subgrid eddies, and thus $\frac{d}{dt} \langle Z \rangle = -\langle \Pi_Z \rangle$. Combining it with $\frac{d}{dt} \langle e \rangle = \langle \Pi_E \rangle$ (Eq. (5)) and (A1), we obtain:

$$\langle \Pi_E \rangle = \frac{d}{dt} \langle e \rangle = \frac{\bar{\Delta}^2}{12} \cdot \frac{d}{dt} \langle Z \rangle = -\frac{\bar{\Delta}^2}{12} \langle \Pi_Z \rangle. \quad (\text{A2})$$

Appendix B Eliminating numerical errors with explicit filtering approach

The discretization errors may be an important source of discrepancies between a priori and a posteriori performance. As an example of numerical effects we refer to works of Bachman et al. (2017); Maulik and San (2017c); Guan, Chattopadhyay, et al. (2022), where the accumulation of energy near the grid scale is shown for dynamic models. In this section, we apply the explicit filtering approach to reduce the role of numerical errors (Gullbrand & Chow, 2003). The main idea of explicit filtering consists in considering the grid step of the coarse model Δ_g and filter width $\bar{\Delta}$ as independent parameters. Fixing the filter width $\bar{\Delta}$ and enlarging the $FGR = \bar{\Delta}/\Delta_g$, it is possible to eliminate the discretization errors from the LES equation (3).

In Figure B1 we show the energy spectrum in a posteriori experiments at a fixed filter width and enlarging FGR (and corresponding grid resolution). At low

resolution ($FGR = 2$) we observe a build-up of energy density near the grid scale, and at larger FGRs coarse models converge to the filtered solution. There is a tradeoff between the strength of discretization errors and the number of directly simulated degrees of freedom (Lund, 1997, 2003; Bose et al., 2010; Sarwar et al., 2017). We use as small FGR as possible to better utilize the grid resolution, but large enough to reduce the role of discretization errors: a suitable choice is $FGR = \sqrt{6}$. It is also the maximum allowable FGR to use 3-point discrete filter defined in Eq. (23). We note that the optimal FGR depends on the hydrodynamic solver and can change in other configurations. The optimal FGR for mixed models (DMM and DMM+Reynolds) at all filter widths is $FGR = \sqrt{6}$, and DSM can be used with $FGR = 2$. For convenience, we use $FGR = \sqrt{6}$ everywhere.

Data Availability Statement

The software of the barotropic model in C++, QG model in Python and NEMO model in Fortran with implemented parameterizations are available via Zenodo (P. Perezhgin & Glazunov, 2023), where we also provide simulation data and Figure plotting functions.

Acknowledgments

An analysis of high-resolution simulations (Sections 2 and 3) was carried out with the financial support of the Russian Science Foundation (project 21-71-30023). Development of subgrid closures (Sections 4 and 5) was supported by the Moscow Center of Fundamental and Applied Mathematics at INM RAS (with the Ministry of Education and Science of the Russian Federation, Agreement 075-15-2022-286).

We are grateful to Laure Zanna, Fabrizio Falasca, Gordey Goyman, Abigail Bodner, Elizabeth Yankovsky, Adam Subel and Dhruv Balwada for insightful discussions and help with the manuscript, and to Andrew Ross for help with implementation into the pyqg model.

References

- Abernathy, R., Rocha, C. B., Ross, A., Jansen, M., Li, Z., Poulin, F. J., ... Tobias (2022, May). *pyqg/pyqg: v0.7.2*. Zenodo. Retrieved from <https://doi.org/10.5281/zenodo.6563667> doi: 10.5281/zenodo.6563667
- Adcroft, A., Anderson, W., Balaji, V., Blanton, C., Bushuk, M., Dufour, C. O., ... others (2019). The gfdl global ocean and sea ice model om4. 0: Model description and simulation features. *Journal of Advances in Modeling Earth Systems*, *11*(10), 3167–3211.
- Anstey, J. A., & Zanna, L. (2017). A deformation-based parametrization of ocean mesoscale eddy reynolds stresses. *Ocean Modelling*, *112*, 99–111.
- Arakawa, A. (1997). Computational design for long-term numerical integration of the equations of fluid motion: Two-dimensional incompressible flow. part i. *Journal of computational physics*, *135*(2), 103–114.
- Bachman, S. D. (2019). The gm+ e closure: A framework for coupling backscatter with the gent and mcwilliams parameterization. *Ocean Modelling*, *136*, 85–106.
- Bachman, S. D., Anstey, J. A., & Zanna, L. (2018). The relationship between a deformation-based eddy parameterization and the lans- α turbulence model. *Ocean Modelling*, *126*, 56–62.
- Bachman, S. D., Fox-Kemper, B., & Pearson, B. (2017). A scale-aware subgrid model for quasi-geostrophic turbulence. *Journal of Geophysical Research: Oceans*, *122*(2), 1529–1554.

- Bardina, J., Ferziger, J., & Reynolds, W. (1980). Improved subgrid-scale models for large-eddy simulation. In *13th fluid and plasmadynamics conference* (p. 1357).
- Bardino, J., Ferziger, J. H., & Reynolds, W. C. (1983). Improved turbulence models based on large eddy simulation of homogeneous, incompressible turbulent flows. *Stanford Univ. Report*.
- Batchelor, G. K. (1969). Computation of the energy spectrum in homogeneous two-dimensional turbulence. *The Physics of Fluids*, *12*(12), II-233.
- Bolton, T., & Zanna, L. (2019). Applications of deep learning to ocean data inference and subgrid parameterization. *Journal of Advances in Modeling Earth Systems*, *11*(1), 376–399.
- Borue, V., & Orszag, S. A. (1998). Local energy flux and subgrid-scale statistics in three-dimensional turbulence. *Journal of Fluid Mechanics*, *366*, 1–31.
- Bose, S. T., Moin, P., & You, D. (2010). Grid-independent large-eddy simulation using explicit filtering. *Physics of Fluids*, *22*(10), 105103.
- Bouchet, F. (2003). Parameterization of two-dimensional turbulence using an anisotropic maximum entropy production principle. *arXiv preprint cond-mat/0305205*.
- Buxton, O., Laizet, S., & Ganapathisubramani, B. (2011). The interaction between strain-rate and rotation in shear flow turbulence from inertial range to dissipative length scales. *Physics of Fluids*, *23*(6), 061704.
- Cabanes, C., Lee, T., & Fu, L.-L. (2008). Mechanisms of interannual variations of the meridional overturning circulation of the north atlantic ocean. *Journal of Physical Oceanography*, *38*(2), 467–480.
- Carati, D., Winckelmans, G. S., & Jeanmart, H. (2001). On the modelling of the subgrid-scale and filtered-scale stress tensors in large-eddy simulation. *Journal of Fluid Mechanics*, *441*, 119.
- Chen, S., Ecke, R. E., Eyink, G. L., Rivera, M., Wan, M., & Xiao, Z. (2006). Physical mechanism of the two-dimensional inverse energy cascade. *Physical review letters*, *96*(8), 084502.
- Chen, S., Ecke, R. E., Eyink, G. L., Wang, X., & Xiao, Z. (2003). Physical mechanism of the two-dimensional enstrophy cascade. *Physical review letters*, *91*(21), 214501.
- Chow, F. K., & Moin, P. (2003). A further study of numerical errors in large-eddy simulations. *Journal of Computational Physics*, *184*(2), 366–380.
- Clark, R. A., Ferziger, J., & Reynolds, W. (1979). Evaluation of subgrid-scale models using an. *J. Fluid Mech*, *91*(part 1), 1–16.
- Ferrari, R., & Wunsch, C. (2009). Ocean circulation kinetic energy: Reservoirs, sources, and sinks. *Annual Review of Fluid Mechanics*, *41*, 253–282.
- Fox-Kemper, B., & Menemenlis, D. (2008). Can large eddy simulation techniques improve mesoscale rich ocean models. *Ocean modeling in an eddying regime*, *177*, 319–337.
- Frederiksen, J. S., O’Kane, T. J., & Zidikheri, M. J. (2012). Stochastic subgrid parameterizations for atmospheric and oceanic flows. *Physica Scripta*, *85*(6), 068202.
- Frezat, H., Le Sommer, J., Fablet, R., Balarac, G., & Lguensat, R. (2022). A posteriori learning for quasi-geostrophic turbulence parametrization. *Journal of Advances in Modeling Earth Systems*, *14*(11), e2022MS003124.
- Gent, P. R., & McWilliams, J. C. (1990). Isopycnal mixing in ocean circulation models. *Journal of Physical Oceanography*, *20*(1), 150–155.
- Germano, M. (1986). A proposal for a redefinition of the turbulent stresses in the filtered navier–stokes equations. *The Physics of fluids*, *29*(7), 2323–2324.
- Germano, M. (1992). Turbulence: the filtering approach. *Journal of Fluid Mechanics*, *238*, 325–336.
- Germano, M., Piomelli, U., Moin, P., & Cabot, W. H. (1991). A dynamic subgrid-scale eddy viscosity model. *Physics of Fluids A: Fluid Dynamics*, *3*(7), 1760–

1765.

- Ghosal, S. (1996). An analysis of numerical errors in large-eddy simulations of turbulence. *Journal of Computational Physics*, *125*(1), 187–206.
- Ghosal, S., Lund, T. S., Moin, P., & Akselvoll, K. (1995). A dynamic localization model for large-eddy simulation of turbulent flows. *J. Fluid Mech*, *286*, 229–255.
- Graham, J. P., & Ringler, T. (2013). A framework for the evaluation of turbulence closures used in mesoscale ocean large-eddy simulations. *Ocean Modelling*, *65*, 25–39.
- Grooms, I., Lee, Y., & Majda, A. J. (2015). Numerical schemes for stochastic backscatter in the inverse cascade of quasigeostrophic turbulence. *Multiscale Modeling & Simulation*, *13*(3), 1001–1021.
- Guan, Y., Chattopadhyay, A., Subel, A., & Hassanzadeh, P. (2022). Stable a posteriori les of 2d turbulence using convolutional neural networks: Backscattering analysis and generalization to higher re via transfer learning. *Journal of Computational Physics*, *458*, 111090.
- Guan, Y., Subel, A., Chattopadhyay, A., & Hassanzadeh, P. (2022). Learning physics-constrained subgrid-scale closures in the small-data regime for stable and accurate les. *Physica D: Nonlinear Phenomena*, 133568.
- Guillaumin, A. P., & Zanna, L. (2021). Stochastic-deep learning parameterization of ocean momentum forcing. *Journal of Advances in Modeling Earth Systems*, *13*(9), e2021MS002534.
- Gullbrand, J., & Chow, F. K. (2003). The effect of numerical errors and turbulence models in large-eddy simulations of channel flow, with and without explicit filtering. *Journal of Fluid Mechanics*, *495*, 323.
- Haarsma, R. J., Roberts, M. J., Vidale, P. L., Senior, C. A., Bellucci, A., Bao, Q., ... others (2016). High resolution model intercomparison project (highresmip v1.0) for cmip6. *Geoscientific Model Development*, *9*(11), 4185–4208.
- Hewitt, H. T., Roberts, M., Mathiot, P., Biastoch, A., Blockley, E., Chassignet, E. P., ... others (2020). Resolving and parameterising the ocean mesoscale in earth system models. *Current Climate Change Reports*, 1–16.
- Horiuti, K. (1997). A new dynamic two-parameter mixed model for large-eddy simulation. *Physics of Fluids*, *9*(11), 3443–3464.
- Jansen, M. F., Adcroft, A., Khani, S., & Kong, H. (2019). Toward an energetically consistent, resolution aware parameterization of ocean mesoscale eddies. *Journal of Advances in Modeling Earth Systems*, *11*(8), 2844–2860.
- Jansen, M. F., & Held, I. M. (2014). Parameterizing subgrid-scale eddy effects using energetically consistent backscatter. *Ocean Modelling*, *80*, 36–48.
- Jansen, M. F., Held, I. M., Adcroft, A., & Hallberg, R. (2015). Energy budget-based backscatter in an eddy permitting primitive equation model. *Ocean Modelling*, *94*, 15–26.
- Juricke, S., Bellinghausen, K., Danilov, S., Kutsenko, A., & Oliver, M. (2023). Scale analysis on unstructured grids: Kinetic energy and dissipation power spectra on triangular meshes. *Journal of Advances in Modeling Earth Systems*, *15*(1), e2022MS003280.
- Juricke, S., Danilov, S., Koldunov, N., Oliver, M., & Sidorenko, D. (2020). Ocean kinetic energy backscatter parametrization on unstructured grids: Impact on global eddy-permitting simulations. *Journal of Advances in Modeling Earth Systems*, *12*(1), e2019MS001855.
- Khani, S., & Dawson, C. N. (2023). A gradient based subgrid-scale parameterization for ocean mesoscale eddies. *Journal of Advances in Modeling Earth Systems*, e2022MS003356.
- Khani, S., Jansen, M. F., & Adcroft, A. (2019). Diagnosing subgrid mesoscale eddy fluxes with and without topography. *Journal of Advances in Modeling Earth Systems*, *11*(12), 3995–4015.

- Kraichnan, R. H. (1967). Inertial ranges in two-dimensional turbulence. *The Physics of Fluids*, *10*(7), 1417–1423.
- Kraichnan, R. H. (1976). Eddy viscosity in two and three dimensions. *Journal of the atmospheric sciences*, *33*(8), 1521–1536.
- Layton, W. J., & Rebholz, L. G. (2012). *Approximate deconvolution models of turbulence: analysis, phenomenology and numerical analysis* (Vol. 2042). Springer Science & Business Media.
- Leith, C. (1996). Stochastic models of chaotic systems. *Physica D: Nonlinear Phenomena*, *98*(2-4), 481–491.
- Leith, C. E. (1968). Diffusion approximation for two-dimensional turbulence. *The Physics of Fluids*, *11*(3), 671–672.
- Lévy, M., Klein, P., Tréguier, A.-M., Iovino, D., Madec, G., Masson, S., & Takahashi, K. (2010). Modifications of gyre circulation by sub-mesoscale physics. *Ocean Modelling*, *34*(1-2), 1–15.
- Loose, N., Bachman, S., Grooms, I., & Jansen, M. (2023). Diagnosing scale-dependent energy cycles in a high-resolution isopycnal ocean model. *Journal of Physical Oceanography*, *53*(1), 157–176.
- Lund, T. (1997). On the use of discrete filters for large eddy simulation. *Annual Research Briefs*, 83–95.
- Lund, T. (2003). The use of explicit filters in large eddy simulation. *Computers & Mathematics with Applications*, *46*(4), 603–616.
- Madec, G., Bourdallé-Badie, R., Bouffier, P.-A., Bricaud, C., Bruciaferri, D., Calvert, D., ... others (2017). Nemo ocean engine.
- Mana, P. P., & Zanna, L. (2014). Toward a stochastic parameterization of ocean mesoscale eddies. *Ocean Modelling*, *79*, 1–20.
- Maulik, R., & San, O. (2016). Dynamic modeling of the horizontal eddy viscosity coefficient for quasigeostrophic ocean circulation problems. *Journal of Ocean Engineering and Science*, *1*(4), 300–324.
- Maulik, R., & San, O. (2017a). A dynamic framework for functional parameterisations of the eddy viscosity coefficient in two-dimensional turbulence. *International Journal of Computational Fluid Dynamics*, *31*(2), 69–92.
- Maulik, R., & San, O. (2017b). A novel dynamic framework for subgrid scale parametrization of mesoscale eddies in quasigeostrophic turbulent flows. *Computers & Mathematics with Applications*, *74*(3), 420–445.
- Maulik, R., & San, O. (2017c). A stable and scale-aware dynamic modeling framework for subgrid-scale parameterizations of two-dimensional turbulence. *Computers & Fluids*, *158*, 11–38.
- Meneveau, C., & Katz, J. (2000). Scale-invariance and turbulence models for large-eddy simulation. *Annual Review of Fluid Mechanics*, *32*(1), 1–32.
- Meneveau, C., & Lund, T. S. (1997). The dynamic smagorinsky model and scale-dependent coefficients in the viscous range of turbulence. *Physics of fluids*, *9*(12), 3932–3934.
- Nadiga, B. (2008). Orientation of eddy fluxes in geostrophic turbulence. *Philosophical Transactions of the Royal Society A: Mathematical, Physical and Engineering Sciences*, *366*(1875), 2489–2508.
- Partee, S., Ellis, M., Rigazzi, A., Shao, A. E., Bachman, S., Marques, G., & Robbins, B. (2022). Using machine learning at scale in numerical simulations with smartsim: An application to ocean climate modeling. *Journal of Computational Science*, *62*, 101707.
- Pawar, S., San, O., Rasheed, A., & Vedula, P. (2020). A priori analysis on deep learning of subgrid-scale parameterizations for kraichnan turbulence. *Theoretical and Computational Fluid Dynamics*, *34*(4), 429–455.
- Pearson, B., Fox-Kemper, B., Bachman, S., & Bryan, F. (2017). Evaluation of scale-aware subgrid mesoscale eddy models in a global eddy-rich model. *Ocean Modelling*, *115*, 42–58.

- Perezhogin, P. (2019). Deterministic and stochastic parameterizations of kinetic energy backscatter in the nemo ocean model in double-gyre configuration. In *Iop conference series: Earth and environmental science* (Vol. 386, p. 012025).
- Perezhogin, P., & Glazunov, A. (2023, April). *Dataset for paper Pavel Perezhogin, Andrey Glazunov "Subgrid parameterizations of ocean mesoscale eddies based on Germano decomposition" submitted to JAMES*. Zenodo. Retrieved from <https://doi.org/10.5281/zenodo.7800196> doi: 10.5281/zenodo.7800196
- Perezhogin, P., Zanna, L., & Fernandez-Granda, C. (2023). Generative data-driven approaches for stochastic subgrid parameterizations in an idealized ocean model. *arXiv preprint arXiv:2302.07984*.
- Perezhogin, P. A. (2020). Testing of kinetic energy backscatter parameterizations in the nemo ocean model. *Russian Journal of Numerical Analysis and Mathematical Modelling*, 35(2), 69–82.
- Porté-Agel, F., Meneveau, C., & Parlange, M. B. (2000). A scale-dependent dynamic model for large-eddy simulation: application to a neutral atmospheric boundary layer. *Journal of Fluid Mechanics*, 415(ARTICLE), 261–284.
- Ross, A., Li, Z., Perezhogin, P., Fernandez-Granda, C., & Zanna, L. (2023). Benchmarking of machine learning ocean subgrid parameterizations in an idealized model. *Journal of Advances in Modeling Earth Systems*, 15(1), e2022MS003258.
- Sagaut, P. (2006). *Large eddy simulation for incompressible flows: an introduction*. Springer Science & Business Media.
- Sagaut, P., & Grohens, R. (1999). Discrete filters for large eddy simulation. *International Journal for Numerical Methods in Fluids*, 31(8), 1195–1220.
- Salmon, R. (1978). Two-layer quasi-geostrophic turbulence in a simple special case. *Geophysical & Astrophysical Fluid Dynamics*, 10(1), 25–52.
- San, O. (2014). A dynamic eddy-viscosity closure model for large eddy simulations of two-dimensional decaying turbulence. *International Journal of Computational Fluid Dynamics*, 28(6-10), 363–382.
- San, O., Staples, A. E., & Iliescu, T. (2013). Approximate deconvolution large eddy simulation of a stratified two-layer quasigeostrophic ocean model. *Ocean Modelling*, 63, 1–20.
- Sarwar, M., Cleary, M., Moinuddin, K., & Thorpe, G. (2017). On linking the filter width to the boundary layer thickness in explicitly filtered large eddy simulations of wall bounded flows. *International Journal of Heat and Fluid Flow*, 65, 73–89.
- Skamarock, W. C., Klemp, J. B., Dudhia, J., Gill, D. O., Barker, D. M., Wang, W., & Powers, J. G. (2008). *A description of the advanced research wrf version 3. ncar technical note-475+ str* (Tech. Rep.).
- Smagorinsky, J. (1963). General circulation experiments with the primitive equations: I. the basic experiment. *Monthly weather review*, 91(3), 99–164.
- Stolz, S., Adams, N. A., & Kleiser, L. (2001). An approximate deconvolution model for large-eddy simulation with application to incompressible wall-bounded flows. *Physics of fluids*, 13(4), 997–1015.
- Sullivan, P. P., Horst, T. W., Lenschow, D. H., Moeng, C.-H., & Weil, J. C. (2003). Structure of subfilter-scale fluxes in the atmospheric surface layer with application to large-eddy simulation modelling. *Journal of Fluid Mechanics*, 482, 101–139.
- Thuburn, J., Kent, J., & Wood, N. (2014). Cascades, backscatter and conservation in numerical models of two-dimensional turbulence. *Quarterly Journal of the Royal Meteorological Society*, 140(679), 626–638.
- Vallis, G. K. (2017). *Atmospheric and oceanic fluid dynamics*. Cambridge University Press.
- Vreman, B., Geurts, B., & Kuerten, H. (1994). On the formulation of the dynamic mixed subgrid-scale model. *Physics of Fluids*, 6(12), 4057–4059.

- Winckelmans, G. S., Wray, A. A., Vasilyev, O. V., & Jeanmart, H. (2001). Explicit-filtering large-eddy simulation using the tensor-diffusivity model supplemented by a dynamic smagorinsky term. *Physics of Fluids*, *13*(5), 1385–1403.
- Yuan, Z., Xie, C., & Wang, J. (2020). Deconvolutional artificial neural network models for large eddy simulation of turbulence. *Physics of Fluids*, *32*(11), 115106.
- Zanna, L., & Bolton, T. (2020). Data-driven equation discovery of ocean mesoscale closures. *Geophysical Research Letters*, *47*(17), e2020GL088376.
- Zanna, L., Mana, P. P., Anstey, J., David, T., & Bolton, T. (2017). Scale-aware deterministic and stochastic parametrizations of eddy-mean flow interaction. *Ocean Modelling*, *111*, 66–80.